Jpn. J. Appl. Phys. Vol. 42 (2003) pp. 3633–3640
Part 1, No. 6A, June 2003

Heavy-Particle Hybrid Simulation of a High-Voltage Glow Discharge in Helium

P. HARTMANN, H. MATSUO[1], Y. OHTSUKA[1], M. FUKAO[1], M. KANDO[1] and Z. DONKÓ

Research Institute for Solid State Physics and Optics of the Hungarian Academy of Sciences, H-1525 Budapest, P.O. Box 49, Hungary
[1]*Department of Electrical and Electronic Engineering, Shizuoka University, Johoku 3-5-1, Hamamatsu 432-8561, Japan*

(Received December 18, 2002; accepted for publication February 6, 2003)

A high-voltage glow discharge — operated at several thousand Volts — is described by a hybrid model in which we apply kinetic simulation for the fast electrons and fast heavy particles (He^+ ions and neutral atoms). In the model we take into account the increase of the gas temperature, and calculate the apparent secondary electron yield at the cathode from the flux-energy distributions of heavy particles. The results of the simulations show that electron production at the cathode is dominated by the impact of fast neutral atoms (ejecting ≈75% of the primary electrons) and that ionization of the gas atoms by fast heavy particles contributes significantly to the ionization balance of the discharge. A fair agreement is obtained between measured and calculated electrical characteristics and potential distributions, and the calculations confirm the existence of the high-energy electron beam observed experimentally. [DOI: 10.1143/JJAP.42.3633]

KEYWORDS: glow discharge, discharge simulation, hybrid modeling, heavy-particle processes, electron beam

1. Introduction

The phenomena taking place in abnormal DC glow discharges — usually operating in the ~Torr pressure range at a voltage of few hundred Volts — have thoroughly been investigated theoretically using different approaches during the past decades.[1–5)] On the other hand, low-pressure glow discharges operating at more extreme conditions, at voltages of several thousand volts, have rarely been studied by self-consistent models. Such discharges have important applications, *e.g.* as high-current electron guns. The experimental investigations[6–8)] of the discharge arrangement studied in this paper (equipped with a concave cathode) have indeed been motivated by this application. The experimental discharge arrangement consists of parallel ≈10 cm-diameter disk electrodes made of aluminium, to minimize cathode sputtering. The discharge has been operated in helium at pressures between 3 Pa and 30 Pa, electrode separations of 20–30 cm, and voltages ranging from 1 kV to 5 kV. The voltage–current–pressure characteristics of the discharge, the potential distribution in the gap, and the energy distribution of fast electrons at the anode have been determined experimentally.[6–8)] Subsequently, measurements of the temperature of the electrodes have also been carried out.[9)] The experiments have also shown that the properties of the discharges with plane and concave cathodes are very similar, except for the focusing of the beam of fast electrons in the case of the concave cathode.

In this paper we present a simulation study of this high-voltage glow discharge.[6–8)] The aim of the present study is to obtain information about the importance of individual elementary processes and about the self-maintenance mechanism of the discharge (processes of charge reproduction), through self-consistent simulations.

In noble gas discharges operating at low discharge voltages (200–300 V) the charge reproduction may be attributed to a good approximation to electron-impact ionization and secondary electron emission from the (cold) cathode due to impact of positive ions. In fact, models based on this simplification have successfully been applied in studies of many different types of discharges during the last decade. Meanwhile, it has also been realized that at higher voltages (600–800 V, typical *e.g.* for glow discharge cells used in analytical spectroscopy[10,11)]) additional processes — *e.g.* ion-impact ionization — also contribute to the charge production.

Regarding the self-maintenance of the discharges, studies of breakdown conditions and low-current discharges in argon gas, carried out by Phelps and Petrović,[12)] have shown that at high reduced electric fields $E/n \geq 10$–20 kTd (1 Td = 10^{-21} Vm^2, E is the electric field and n is the gas density) fast neutral atoms also contribute significantly to the electron emission from the cathode. Fast neutral atoms originate from charge and momentum transfer collisions between noble gas ions/atoms and thermal buffer gas atoms. While a positive ion traverses the cathode sheath it may create several fast atoms (which can create additional fast atoms through momentum transfer collisions). This way the flux of fast atoms may significantly exceed the flux of ions at the cathode. (Due to their high flux, fast atoms may also dominate the sputtering of the cathode.[13,14)])

Earlier studies of breakdown in helium gas have indicated that the importance of fast-atom-induced secondary electron emission exceeds that induced by He^+ ions at reduced electric fields $E/n \geq 20$ kTd.[15)] Taking into account that in our high voltage discharge the reduced electric field at the cathode may reach values as high as ~60 kTd,[6)] we expect fast-atom-induced electron emission to be an important process, unlike in low-voltage discharges. We also expect that ionization by fast heavy particles becomes important in the cathode sheath due to the high values of E/n. The importance of these processes is analyzed in our model by including/neglecting them in the simulation. Besides the processes discussed above we also investigate the effect of gas heating as well as the effect of the reflection of fast electrons from the anode of the discharge.

In §2, the simulation model is described in detail. Section 3 presents the modeling results and compares them with the experimental data where available. Section 4 gives the conclusions of the work.

2. Simulation model

Our simulations are based on a hybrid model[10,11,16–22)] that combines the fluid description of helium ions and slow electrons with the Monte Carlo simulation of fast plasma species: fast electrons, helium ions and fast neutral atoms.

The model is one-dimensional in space, but the Monte Carlo simulation uses all the three velocity coordinates.

In the cathode fall region electrons acquire high energy. As their free path can be comparable to the length of the cathode sheath, the transport of fast electrons is non-hydrodynamic,[23] only a kinetic description (*e.g.* the solution of the Boltzmann equation[24–29] or Monte Carlo simulation[30,31]) guarantees a correct description of their motion and makes it possible to calculate an accurate ionization source function. For the slow electrons which are no longer able to ionize the gas, the hydrodynamic treatment is sufficiently accurate, so these electrons can be described with a computationally more effective fluid model. In our model we use the usual way — applied in hybrid models — to distinguish between fast and slow electrons.[3,32] We treat the electrons as fast electrons as long as they are able to ionize (their energy is higher or may become higher than the ionization potential of the gas). When they are no longer able to produce any ionization of the gas, they are transferred to the slow electron group.

In our model we also describe the motion of the helium ions and fast neutral atoms in the cathode sheath by Monte Carlo (MC) simulation, in order to calulate the flux-energy distribution of these particles at the cathode surface and the heating power deposited into the gas through collision processes (see later).

In summary, we use Monte Carlo simulation for (i) the fast electrons in the whole discharge and (ii) for positive ions and fast neutral atoms in the cathode sheath. The fluid model covers the whole discharge region, although, as it will be shown later, no slow electrons exist in the cathode sheath. As for the ions, the Monte Carlo simulation is used to obtain their energy distribution at the cathode, while their density is calculated in the fluid model.

In hybrid models the 'apparent' secondary electron emission coefficient γ (the ratio of the electron current to the ion current at the cathode) is usually defined as an input parameter. Until recently most of the models have used a constant value for γ, even for a wide range of discharge conditions. Recent studies have, however, shown that γ (and consequently the calculated discharge characteristics) may depend considerably on the actual discharge conditions.[12,22,33,34] Because of this, in our present model we calculate γ from the flux-energy distributions of fast He^+ ions and fast He atoms at the cathode surface. We assume that these two species play the dominant role in secondary electron emission.

Additionally, in our model we take into account the temperature increase of the gas, and calculate the temperature profile between the electrodes in a self-consistent manner. (The temperature increase results in a decreased gas density in the discharge region, whilst the pressure remains constant in the system.) The reflection of fast electrons from the anode is also included in the model, as well as the reflection of fast neutrals from the cathode. Due to the flexibility of the model the effect of individual processes on the results can easily be determined.

2.1 *The fluid model*

The fundamental quantities in the one-dimensional fluid model are the electric potential and the density of slow electrons and He^+ ions. Particle balance for these species is expressed by the continuity equations:

$$\begin{aligned} \frac{\partial n_e}{\partial t} + \frac{\partial \phi_e}{\partial x} &= S_e, \\ \frac{\partial n_i}{\partial t} + \frac{\partial \phi_i}{\partial x} &= S_i, \end{aligned} \tag{1}$$

where n_e and n_i are the electron and ion densities, ϕ_e and ϕ_i are the electron and ion fluxes and S_e and S_i are the source functions of slow electrons and He^+ ions. The fluxes are calculated on the basis of the drift-diffusion approximation:

$$\begin{aligned} \phi_e &= -\mu_e n_e E - \frac{\partial (n_e D_e)}{\partial x}, \\ \phi_i &= \mu_i n_i E - \frac{\partial (n_i D_i)}{\partial x}, \end{aligned} \tag{2}$$

where μ_e and μ_i are the mobilities of electrons and ions, respectively. $E = -\partial V/\partial x$ is the x component of the electric field and V is the potential:

$$\frac{\partial^2 V}{\partial x^2} = -\frac{e}{\varepsilon_0}(n_i - n_e), \tag{3}$$

where e is the elementary charge and ε_0 is the permittivity of free space. The diffusion coefficients D_e and D_i are calculated from the Einstein relation: $D = \mu k_B T$ where k_B is the Boltzmann constant and T is the characteristic energy for the given species. In our calculations we use $k_B T_e = 1\,\mathrm{eV}$[10,11,17,32,35] and $k_B T_i = 0.026\,\mathrm{eV}$. The mobility of electrons and He^+ ions is given by:

$$\mu_e = \frac{1}{3}\frac{T}{p} \times 10^4 \quad \mathrm{cm^2 V^{-1} s^{-1}} \tag{4}$$

and

$$\mu_i = \frac{29.1T}{p}\frac{1}{(1 + (0.034 \times E/p)^{1.26})^{0.41}} \quad \mathrm{cm^2 V^{-1} s^{-1}}, \tag{5}$$

where T is the gas temperature in Kelvin, p is the gas pressure in Torr and E is the electric field strength in V/cm.[36,37]

The $S_i(x)$ and $S_e(x)$ source function are calculated in the MC simulation modules.

2.2 *The Monte-Carlo model*

The motion of energetic particles is traced using MC simulation. In this algorithm random numbers are used to determine the positions and the types of the collisions.

Electrons are traced by MC simulation from the moment of their emission from the cathode until (i) their total (kinetic+potential) energy falls below the ionization potential of the gas, or (ii) they reach the anode. Energetic electrons hitting the anode can also be absorbed or reflected and can initiate secondary electron emission.

Positive ions and fast neutral atoms in the cathode sheath are traced (i) until they reach the cathode, or (ii) in the case of the fast atoms, their energy falls below an energy limit of $27/2 k_B T$ that is used to distinguish between fast and thermal atoms.[38] When the energy of a fast atom becomes less than this threshold, the particle is no longer traced, and its energy is transferred to the power source term for the gas heating calculation.[38] The fast heavy particles that reach the cathode

surface can be absorbed or reflected with a certain probability and with a fraction of their kinetic energy.[39)]

The trajectory of a particle between successive collisions is followed by direct integration of the equation of motion:

$$m\frac{\mathrm{d}^2\mathbf{r}}{\mathrm{d}t^2} = q\mathbf{E}, \tag{6}$$

where m and q are the mass and the charge of the particle, respectively. The free path is assigned statistically and the positions of the collisions are calculated from

$$\int_{s_0}^{s_1} n\sigma[\varepsilon(s)]\mathrm{d}s = -\ln(1-R_{01}), \tag{7}$$

where s_0 is the position of the last collision and s_1 is the position of the next collision measured on the curvilinear abscissa s; n is the background gas density, σ is the sum of cross sections of all possible elementary processes, ε is the kinetic energy of the particle and R_{01} is a random number with uniform distribution in the [0,1) interval.[31)]

The types of the collisions which occur after the free flights are chosen statistically, taking into account the values of cross sections of different processes at the energy of the colliding particle.

2.3 *Elementary processes*

In the gas phase we take into account elastic, excitation and ionization collision processes of electrons, He^+ ions and fast He atoms with the background gas. The processes are listed in Table I (with their literature sources indicated) and their cross sections are plotted in Fig. 1(a).

The initial energy of the electrons leaving the cathode is chosen randomly between 0 and 10 eV,[43)] and their initial velocity is set perpendicular to the cathode surface. Some of the primary electrons are backscattered to the cathode, for such electrons we take into account elastic and inelastic reflection/reemission[44)] and absorption at the cathode. The scattering of the electrons in elastic and excitation collisions is assumed to be isotropic. Excitation may occur from the ground level to one of the seven levels or group of levels (2^3S, 2^1S, 2^3P, 2^1P, 3SPD, 4SPD, 5SPD). The cross sections of electron impact processes are taken from.[36)]

He^+ ions in the gas are accelerated towards the cathode. Gaining energy from the electric field these particles are able to take part in elastic and inelastic collision processes listed in Table I. Elastic collision processes are important sources of fast neutral atoms. The ions as well as the fast neutrals are also able to excite and ionize the background gas atoms. The cross section of the isotropic part of the elastic He^++He collisions (Q_i) is taken from Phelps,[45)] while the charge transfer cross section (backward part of elastic scattering, Q_b) is obtained from the momentum transfer cross section (Q_m) as $Q_b = (Q_m - Q_i)/2$.[46)] In isotropic collisions the scattering and azimuth angles are chosen to reflect isotropic scattering in the center-of-mass (COM) frame. The energy sharing of the collision partners is determined from the scattering angles.[10)] The cross section of the elastic He(f)+He collision in isotropic approximation is $Q_i^a = (3/2)Q_v$, where Q_v is the viscosity cross section.[45)]

Table I. Gas-phase elementary processes considered in the model.

No.	Process	Process name	Reference
1.	e+He → e+He	elastic collision	36
2.	e+He → e+He*	excitation (7 levels)	36
3.	e+He → e+He^+	ionization	36
4.	He^++He → He^++He(f)	elastic collision (isotropic part)	45
5.	He^++He → He^++He(f)	elastic collision (backward part)	45
6.	He^++He → He^++He*(f)	excitation	40
7.	He^++He → 2He^++e	ionization	41
8.	He(f)+He → He(f)+He(f)	elastic collision	45
9.	He(f)+He → He(f)+He*	excitation	42
10.	He(f)+He → He(f)+He^++e	ionization	49

Note: He* and He(f) denote excited and fast helium atoms, respectively.

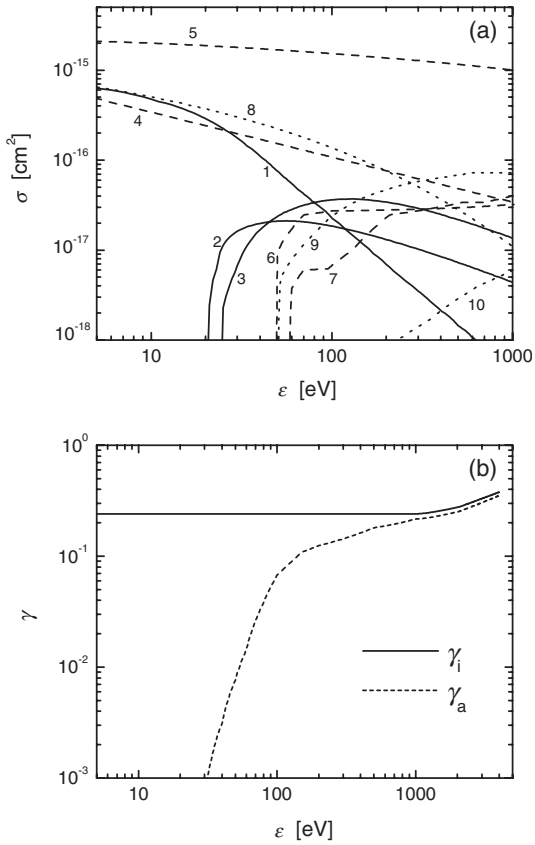

Fig. 1. Model input data: (a) Cross sections of the elementary processes in the discharge (solid lines: electron cross sections, dashed lines: He^+ cross sections, dotted lines: fast neutral cross sections). The numbering of the curves corresponds to the processes listed in Table I; (b) Ion and fast atom induced electron emission yield for the He+Al system.

The MC simulation of the fast heavy particles in the cathode fall makes it possible to calculate the apparent secondary emission coefficient at the cathode from the flux-energy distributions of fast ions and atoms,[22)] this way providing information about the maintenance mechanism of the discharge. Using energy-dependent electron yield values for positive ions $\gamma_i(\varepsilon)$ and fast atoms $\gamma_a(\varepsilon)$ the apparent secondary electron yield can be calculated as:

$$\gamma = \frac{\sum_{k=1}^{N_i}\gamma_i(\varepsilon_k) + \sum_{k=1}^{N_a}\gamma_a(\varepsilon_k)}{N_i}, \tag{8}$$

where N_i and N_a are the number of ions and fast atoms arriving to the cathode, and ε_k is the energy of the k-th ion or atom. In a self-sustained discharge this apparent γ is equal to

the ratio of electron and ionic current at the cathode surface.

The $\gamma_i(\varepsilon)$ and $\gamma_a(\varepsilon)$ functions used as input data of our model are shown in Fig. 1(b). For $\gamma_i(\varepsilon)$ [$He^+ \rightarrow$ Al impact] the data of Hasselkamp[47,48] are used. At energies below 1200 eV $\gamma_i(\varepsilon)$ is assumed to be constant. Due to the lack of data in the literature for $\gamma_a(\varepsilon)$ [He(f) $\rightarrow$ Al impact] we assumed that the ratio of $\gamma_a(\varepsilon)$ to $\gamma_i(\varepsilon)$ is the same as the ratio of secondary yields of He(f) $\rightarrow$ Cu and $He^+ \rightarrow$ Cu processes, for which experimental data are available.[49] These data correspond to cathode surfaces under laboratory conditions. It is noted that the secondary electron yields measured under ultra-high vacuum conditions are significantly different and cannot directly be applied for glow discharge simulations.[12]

2.4 *Gas heating*

Modeling studies of abnormal glow discharges[35,38] have indicated that at current densities in the mA/cm^2 range the increase of gas temperature may already be considerable. While our discharge operates at lower current density, due to the higher voltage and lower pressure it is appropriate to take into account gas-heating effects.

Energy to the background gas is transferred mainly from the thermalization of fast neutral atoms created in collisions between fast heavy particles and buffer gas atoms. The gas temperature distribution $T_g(x)$ is calculated similarly to that described by Revel *et al.*[35] The heat conductivity equation:

$$\frac{d^2T_g(x)}{dx^2} + \frac{P(x)}{\kappa} = 0, \tag{9}$$

where $P(x)$ is the gas heating source term and $\kappa = 0.143\,\mathrm{Wm^{-1}K^{-1}}$ is the thermal conductivity of helium gas, is solved with the boundary conditions:[35]

(1) given anode temperature T_a, and

(2) specified temperature gradient in front of the cathode:

$$\kappa \left|\frac{dT}{dx}\right|_{\text{cathode}} = \frac{2\alpha}{2-\alpha} C_p m_p \Delta T_s \frac{n_s v_s}{4}, \tag{10}$$

where α is the thermal accommodation coefficient, C_p is the specific heat of the gas at constant pressure, m_p, n_s and v_s are the mass, the density, and the average thermal velocity of He atoms in front of the cathode, respectively, and ΔT_s is the "temperature jump" at the cathode surface (the difference of the cathode temperature T_c and the gas temperature in front of the cathode T_s).

The thermal accommodation coefficient α describes the extent of energy exchange between the cathode and the slow particles colliding with it. At $\alpha = 1$ the backscattered particles attain the temperature of the cathode, while at $\alpha = 0$ no energy exchange occurs during the reflection. In our calculations we used the value $\alpha = 0.5$. The T_c and T_a values for the different discharge conditions are taken from experiments[9] and are used as input data of the model.

For the interaction of fast particles (that can have up to several thousand eV energy in the cathode sheath) with the cathode surface different assumptions are used in the modeling literature. In the present model it is assumed that the particles are reflected from the cathode with a fraction of their kinetic energy.

The gas heating term $P(x)$ — arising from the thermalization of fast heavy particles — is calculated according to the procedures described by Bogaerts *et al.*[38] He^+ ions as well as fast neutral atoms [He(f)] originating from He^++He and He(f)+He elastic collisions are traced by the Monte Carlo model. When these species participate in collision processes they transfer energy to the atoms of the buffer gas. The fast atoms finally distribute their energy to several additional atoms which leads to the heating of the background gas. The simulation makes it possible to obtain the spatial distribution of collision events and the amount of energy transferred to the gas, which — after proper normalization — gives the $P(x)$ gas heating source term.

3. Results

The results of the calculations are presented for a constant electrode separation $L = 28$ cm, a voltage of $V = 4000$ V, and for three values of current: $I = 1$ mA, 5 mA, and 20 mA. Due to small uncertainties in pressure measurement in the experiment we adjust the gas pressure in the calculations in a way that the calculated values of current match the experimental ones. Figure 2 shows the measured and calculated current–pressure characteristics of the discharge. The experimental and calculated curves show a similar behavior and are in a reasonable agreement, within $\approx$10%. This deviation is acceptable if we consider the uncertainties of the input data (cross sections, secondary electron yield values). The calculated values of the pressure for the three current values indicated above are $p = 27$ mTorr, 38 mTorr, and 57 mTorr (the experimental values are 29 mTorr, 42 mTorr, and 61 mTorr). Figure 2 also shows current–pressure characteristics obtained by neglecting different elementary processes. This additional information is discussed later.

Figure 3(a) shows the potential distribution between the electrodes, for $I = 1$, 5, and 20 mA. The $V(x)$ curves clearly show the cathode sheath — negative glow structure of the discharges operated at 5 mA and 20 mA. For these conditions the potential distribution is closely parabolic at the cathode side of the gap. The cathode sheath has a length

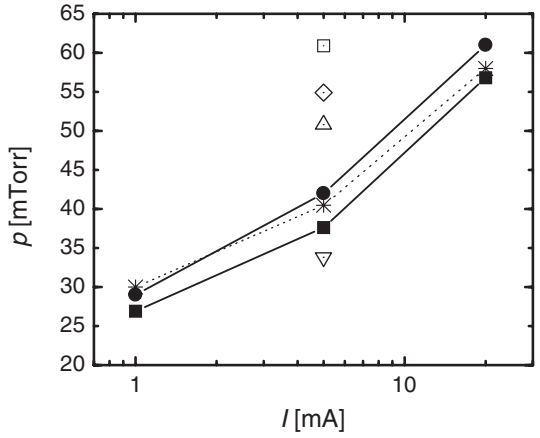

Fig. 2. Measured (●) and calculated current – pressure characteristics of the investigated discharges; $V = 4000$ V, $L = 28$ cm and $I = 1$, 5, and 20 mA. "Full simulation": ■, neglecting gas heating: ▽, neglecting ion-impact ionization: △, neglecting reflection of fast electrons from the anode: ◇, neglecting all processes of fast atoms: □. Full simulation including wall-loss of fast atoms: ∗.

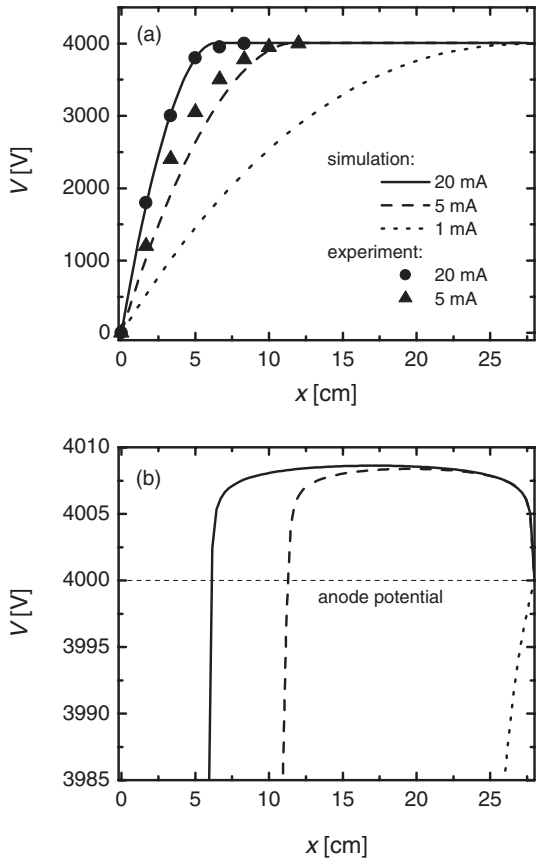

Fig. 3. (a) Calculated (lines) and measured (symbols) potential distribution in the discharges at $V = 4000$ V, $L = 28$ cm and $I = 1$, 5, and 20 mA. The cathode is situated at $x = 0$ cm, while the anode is at $x = 28$ cm. (b) Potential distribution in the negative glow. (The horizontal dashed line shows the anode potential.)

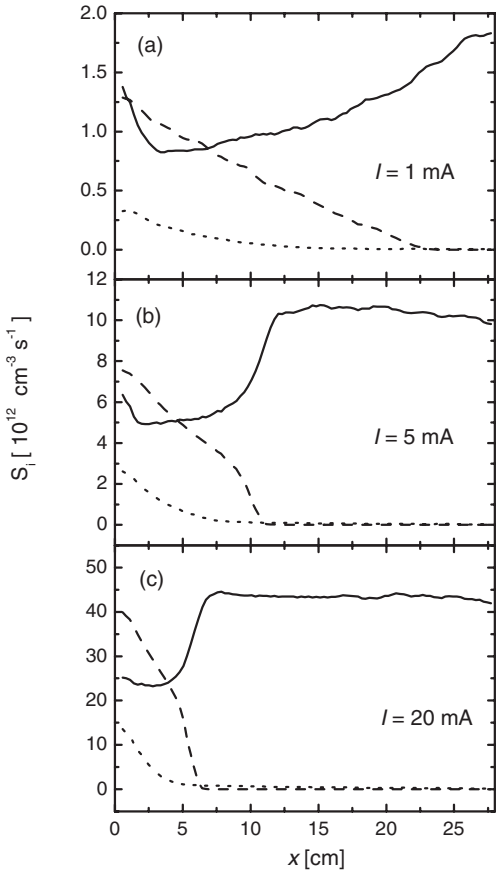

Fig. 4. Contribution of electron impact (————), fast ion impact (– – –) and fast atom impact (· · ·) processes to the ionization source. ($V = 4000$ V, $L = 28$ cm and $I = 1$, 5 and 20 mA.)

(determined from the extrapolation of the linearly falling part of $E(x)$ to zero field), $d_c \approx 10$ cm and 6 cm, respectively, for the above values of the current. The space beyond the cathode sheath is filled by the negative glow. At $I = 1$ mA the cathode sheath occupies the whole discharge region, the negative glow is not formed.

At the higher values of the current (5 mA and 20 mA) the simulations show the existence of an electric field reversal in the negative glow part of the discharge, the electric field at the anode is slightly negative. The enlarged part of the potential distribution as plotted in Fig. 3(b) shows a plasma potential $\approx$8 V higher than the anode potential. The position of the field reversal (which coincides with the position of the maximum of the potential) is located at $d_f = 19.7$ cm, and 17.2 cm, respectively, for $I = 5$ and 20 mA. We find that for these values of the current the field reversal position is situated halfway between the position of the sheath–glow boundary and the anode. This behavior is in excellent agreement with the predictions of the analytical model of Boeuf and Pitchford.[50] According to their model the field reversal position, d_f, depends only on the electrode distance L, the length of the cathode sheath d_c and the energy relaxation length of the fast electrons λ:

$$\frac{d_f - d_c}{L - d_c} = -\Lambda \ln\left[\Lambda(1 - e^{-1/\Lambda})\right], \qquad (11)$$

where $\Lambda = \lambda/(L - d_c)$. As it will be shown later, the energy relaxation length of the electrons in our discharge is much longer than the electrode distance, $\lambda \gg L$. Consequently $(d_f - d_c)/(L - d_c) \approx 0.5$, and $d_f \approx (L + d_c)/2$, in agreement with our observations.

Experimental data for the potential, measured by emissive probe technique,[7] for the $I = 5$ and 20 mA cases are also plotted in Fig. 3(a). The results of the calculations are in a fair agreement with the experimental data.

The ionization source functions $S_i(x)$, shown in Fig. 4 for the 1, 5, and 20 mA cases, indicate that apart from the electron impact ionization, there is a significant source of ions due to the ionizing collisions between fast heavy particles and the background He atoms. Moreover, this latter part of the ionization source peaks near the cathode. This way the electrons created through this channel have a possibility to create additional electron avalanches, just like the primary electrons do. This effect strongly enhances the overall ionization rate in the discharge. The importance of heavy particle ionization decreases with increasing discharge current. At 1 mA 32% of the ions are created in heavy particle processes. This ratio drops to 14% at 20 mA. In lower voltage glow discharges the electron impact ionization rate (and similarly the electron impact excitation rate) peaks at (or very near) the cathode sheath — negative glow boundary[51] and decays nearly exponentially beyond this point.[52] In the present case we observe only a very slow (if any) decay of S_i in the negative glow. This shows that the gap is too narrow for the electrons to deposit their energy

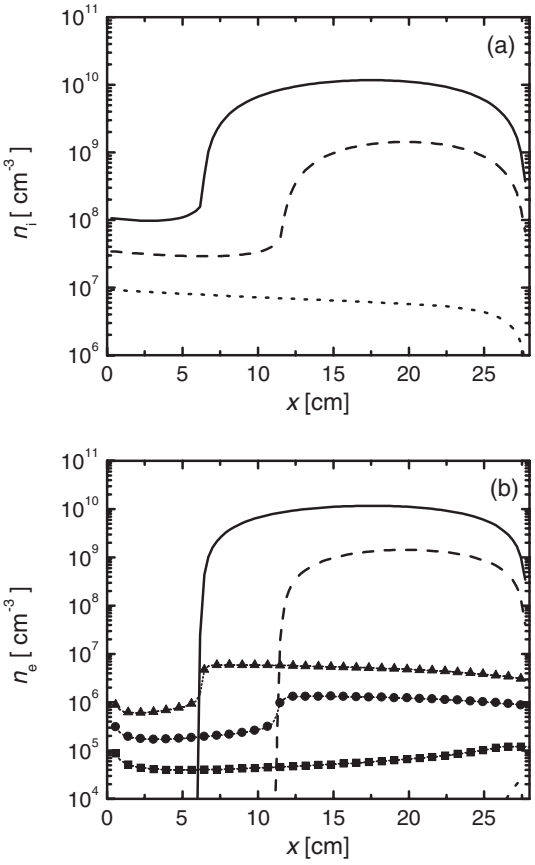

Fig. 5. (a) He^+ ion density and (b) slow electron density distribution, ··· $I = 1$ mA; – – – $I = 5$ mA; ———— $I = 20$ mA ($V = 4000$ V and $L = 28$ cm). Symbols in (b): fast electron density: ■ $I = 1$ mA; ● $I = 5$ mA; ▲ $I = 20$ mA.

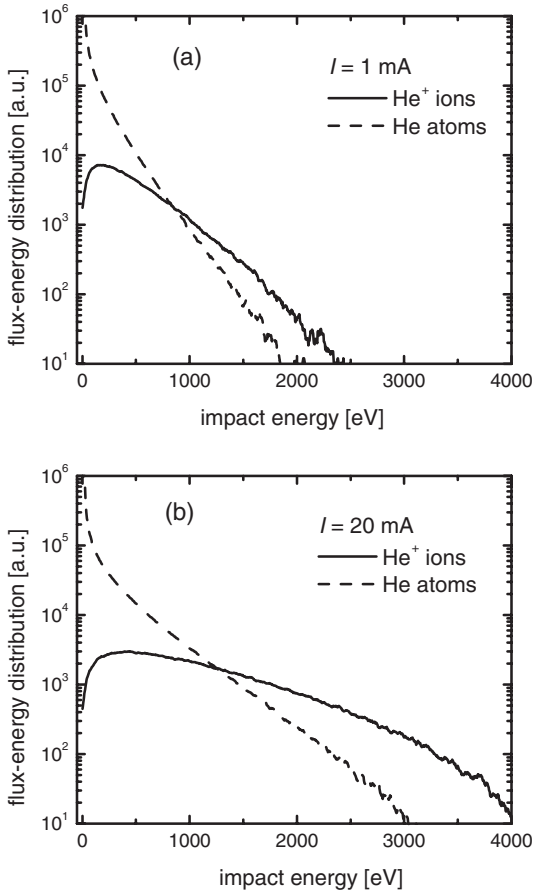

Fig. 6. Flux-energy distribution of heavy particles (He^+ ions and fast neutrals) at the cathode surface for $I = 1$ mA and 20 mA ($V = 4000$ V).

before reaching the anode, i.e. their energy relaxation length is much longer compared to the electrode distance.

Figure 5 shows the density distribution of charged particles in the discharge gap. The two different regions can clearly be distinguished at $I = 5$ mA and 20 mA. The ion density is relatively low in the drift dominated cathode sheath. In this region the density of slow electrons is negligible [as shown in Fig. 5(b)] as they cannot enter this region from the negative glow, due to the high electric field gradient. Figure 5(b) also shows the density of fast electrons (obtained from their MC simulation). In the negative glow the density of slow electrons exceeds the density of fast electrons by about three orders of magnitude. At the lowest current investigated ($I = 1$ mA) a fairly uniform ion and electron density is present in the discharge gap. The ion density exceeds the density of fast electrons by two orders of magnitude.

The flux-energy distribution of fast heavy particles is plotted in Fig. 6 for $I = 1$ mA and 20 mA. As a He^+ ion passes through the cathode sheath it may participate in a number of charge (or monentum) exchange collisions. In each of these collisions a fast atom can be created. These fast atoms further distribute their energy to several other atoms, consequently the total flux of fast neutrals to the cathode is significantly higher compared to that of the He^+ ions. The energy distributions show a higher number of energetic species at 20 mA. This is explained by the lower value of pd_c in this case (being 47 Pa cm) compared to $pd_c \approx 100$ Pa cm in the case of $I = 1$ mA. (The number of collisions in the cathode sheath is approximately proportional to pd_c).

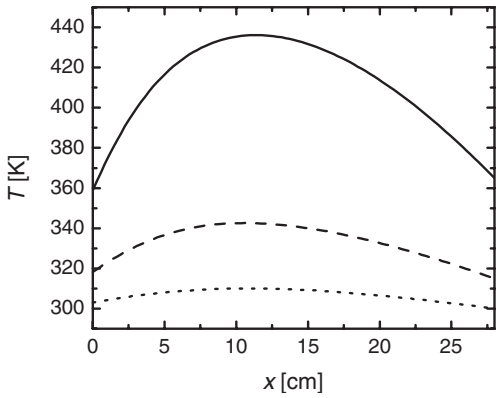

Fig. 7. Gas temperature distribution in the discharge gap, ··· $I = 1$ mA; – – – $I = 5$ mA; ———— $I = 20$ mA ($V = 4000$ V and $L = 28$ cm).

In Fig. 7 the temperature distribution of the background He gas is shown for the three discharges $I = 1$, 5, and 20 mA. The temperatures of the cathode for these conditions are 300 K, 310 K, and 340 K, respectively, while the anode temperatures are 300 K, 315 K, and 365 K.[9] The temperature increase of the electrodes and of the gas becomes significant as the discharge current increases. A temperature increase of more than 40% — in comparison with room temperature — can be observed in the 20 mA case. This temperature rise

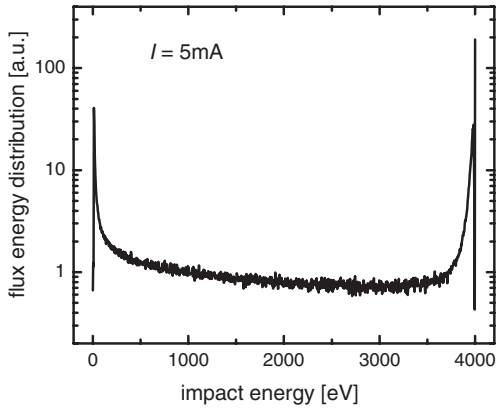

Fig. 8. Flux-energy distribution of fast electrons reaching the anode ($V = 4000\,\mathrm{V}$, $L = 28\,\mathrm{cm}$ and $I = 5\,\mathrm{mA}$.)

already has important consequences to the discharge processes due to the reduction of the gas density thereby modifying the free path of the particles.

As primary electrons leave the cathode they are soon accelerated to energies far exceeding the energy corresponding to the peak of inelastic cross sections. As a consequence of this many of the primary electrons fly through the cathode sheath and even the whole discharge gap without inelastic energy losses. Figure 8 shows the energy spectrum of the fast electrons reaching the anode for the $I = 5\,\mathrm{mA}$ discharge. (This spectrum does not include the flux of slow electrons treated in the fluid model.) The energy spectrum shows a pronounced peak at the energy (4000 eV) corresponding to the full cathode fall voltage (beam electrons), in agreement with the experiments.[6] Approximately 35% of the fast electrons at the anode have an energy higher than 3900 eV for all investigated discharge conditions. Consequently, the electron-reflecting properties of the anode material strongly influence the ionization rate in the discharge.

The apparent secondary electron emission coefficient at the cathode is found to be $\gamma \approx 0.96$ for the investigated discharge conditions. This high value of γ includes a contribution of fast atoms; for all of our discharge conditions investigated ≈75% of the electrons are emitted due to fast atom impact. The ratio of the fluxes of fast neutral atoms and ions at the cathode varies from about 10 : 1 for 1 mA to 8 : 1 for 20 mA. The secondary electron yield is approximately 0.24 (in all cases) per 'average' ion and 0.072 to 0.097 per fast atom, respectively. According to eq. (8) the contribution of fast atoms to the secondary emission is added to the contribution of the He^+ ions and this results in a high apparent secondary emission yield.

As mentioned in §1, we also investigate the effect of individual elementary processes by including/neglecting them in the simulation. The results of this study are illustrated for the $I = 5\,\mathrm{mA}$ case. As some of these changes influence drastically the ionization balance of the discharge, we have decided to change the gas pressure and sustain a fixed current during this study. As Fig. 2 shows, "turning off" the gas heating mechanisms the fixed current of 5 mA can be established at 11% lower pressure compared to the pressure obtained in the full simulation. In contrast with this, when we neglect ion-impact ionization, the reflection of fast electrons from the anode of the discharge, or neglecting all processes involving fast atoms, we need to set a gradually increased gas pressure. Without considering the processes of fast atoms the pressure needs to be increased by ≈60% to keep the fixed current of 5 mA. Only this higher pressure can compensate for the loss of charged particle creation by the neglected processes. These results indeed reveal the importance of the selected processes.

Although our model is one-dimensional we have also tested the effect of the discharge tube wall (present in the experiment) on the transport of fast neutral atoms. We have found that taking into account the collisions of fast atoms with the wall reduces their flux to the cathode surface by 20% to 30%, depending on the gas pressure. The effect becomes pronounced at lower pressures where the cathode sheath is long, and is less important when the length of the sheath is less than the diameter of the discharge tube. The wall losses also reduce the contribution of the fast atoms to the secondary electron emission, the apparent electron yield reduces to $\gamma = 0.73$ at 1 mA, and to $\gamma = 0.86$ at 20 mA. As it can be seen in Fig. 2, however, the inclusion of wall losses has relatively little influence on the calculated pressure-current characteristics.

4. Summary

We have investigated thorugh hybrid modeling a high-voltage glow discharge in helium gas. It has been found that several properties of the discharge differ significantly from those of conventional glow discharges operated at voltages of few hundred volts.

Our simulations have shown that in the high-voltage low-pressure helium discharge ($V = 4000\,\mathrm{V}$, $L = 28\,\mathrm{cm}$) investigated:

- a significant part, ≈75% of the electrons is emitted from the cathode due to the impact of fast neutral atoms, originating from heavy-particle collision processes, as predicted by Fukao *et al.*,[6]
- fast ion/atom+He collision processes play a role as additional important sources of ionization,
- there is a significant flux of beam electrons at the anode, in agreement with experimental observations. This observation confirms that such high-voltage discharges can be applied as sources of electron beams and modeling may assist their optimization,
- Heating of the gas and of the electrodes plays an important role, under the discharge conditions investigated.

Acknowledgements

This work has been supported by the Hungarian Science Foundation, Grant OTKA-T-34156.

1) M. Surendra, D. B. Graves and G. M. Jellum: Phys. Rev. A **41** (1990) 1112.
2) A. V. Phelps, Z. Lj. Petrović and B. M. Jelenković: Phys. Rev. E **47** (1993) 2825.
3) A. Fiala, L. C. Pitchford and J. P. Boeuf: Phys. Rev. E **49** (1994) 5607.
4) F. Sigeneger and R. Winkler: Eur. Phys. J. A **19** (2002) 211.
5) A. V. Phelps: Plasma Sources Sci. Technol. **10** (2000) 329.
6) M. Fukao, M. Ishida, Y. Ohtsuka and H. Matsuo: Vacuum **59** (2000) 358.
7) Y. Ohtsuka: unpublished.
8) H. Matsuo, Y. Ohtsuka and M. Fukao: Proc. ESCAMPIG-16/ICRP-5

Conf., Grenoble, France, 2002, Vol. 2, p. 73.
9) H. Matsuo and M. Kando: (2002) unpublished.
10) A. Bogaerts, M. van Straaten and R. Gijbels: Spectrochim. Acta **50B** (1995) 179.
11) A. Bogaerts and R. Gijbels: J. Appl. Phys. **78** (1995) 6427.
12) A. V. Phelps and Z. Lj. Petrović: Plasma Sources Sci. Technol. **8** (1999) R21.
13) A. Bogaerts and R. Gijbels: J. Appl. Phys. **79** (1996) 1279.
14) A. Bogaerts and R. Gijbels: Spectrochim. Acta B **53** (1998) 437.
15) P. Hartmann, Z. Donkó, G. Bánó, L. Szalai and K. Rózsa: Plasma Sources Sci. Technol. **9** (2000) 183.
16) A. Bogaets, R. Gijbels and W. J. Goedheer: Anal. Chem. **68** (1996) 2296.
17) A. Bogaerts: Plasma Sources Sci. Technol. **8** (1999) 210.
18) E. Shidoji, H. Ohtake, N. Nakano and T. Makabe: Jpn. J. Appl. Phys. **38** (1999) 2131.
19) E. Shidoji, N. Nakano and T. Makabe: Thin Solid Films **351** (1999) 37.
20) E. Shidoji, K. Ness and T. Makabe: Vacuum **60** (2001) 299.
21) Z. Donkó: J. Appl. Phys. **88** (2000) 2226.
22) Z. Donkó: Phys. Rev. E **64** (2001) 026401.
23) L. C. Pitchford, J. P. Boeuf, P. Segur and E. Marode: in *Nonequlibrium Effects in Ion and Electron Transport*, ed. J. W. Gallagher (Plenum Press, New York, 1990).
24) H. Tagashira, Y. Sakai and S. Sakamoto: J. Phys. D **10** (1977) 1051.
25) R. Winkler, G. Petrov, F. Sigeneger and D. Uhrlandt: Plasma Sources Sci. Technol. **6** (1997) 118.
26) D. Uhrlandt, M. Schmidt, J. F. Behnke and T. Bindemann: J. Phys. D **33** (2000) 2475.
27) M. Hannemann, P. Hardt, D. Loffhagen, M. Schmidt and R. Winkler: Plasma Sources Sci. Technol. **9** (2000) 387.
28) C. M. Ferreira and J. Loureiro: Plasma Sources Sci. Technol. **9** (2000) 528.
29) I. A. Porokhova, Yu. B. Golubovskii, J. Bretagne, M. Tichy and J. F. Behnke: Phys. Rev. E **63** (2001) 056408.
30) Y. Sakai, H. Tagashira and S. Sakamoto: J. Phys. D **10** (1977) 1035.
31) J. P. Boeuf and E. Marode: J. Phys. D **15** (1982) 2169.
32) J. P. Boeuf and L. C. Pitchford: IEEE Trans. Plasma Sci. **19** (1991) 286.
33) A. V. Phelps, L. C. Pitchford, C. Pédoussat and Z. Donkó: Plasma Sources Sci. Technol. **8** (1999) B1.
34) A. Bogaerts and R. Gijbels: Plasma Sources Sci. Technol. **11** (2002) 27.
35) I. Revel, L. C. Pitchford and J. P. Boeuf: J. Appl. Phys. **88** (2000) 2234.
36) J. P. Boeuf: Phys. Rev. A **36** (1987) 2782.
37) H. Helm and M. T. Elford: J. Phys. B **11** (1978) 3939.
38) A. Bogaerts and R. Gijbels: J. Appl. Phys. **87** (2000) 8334.
39) E. W. Thomas: Oak Ridge Nat. Lab. Report ORNL-6088/V3 (1985) E-10.
40) R. Okasaka, Y. Konishi, Y. Sato and K. Fukuda: J. Phys. B **20** (1987) 3771.
41) H. B. Gilbody and J. B. Hasted: Proc. Roy. Soc. A **240** (1957) 382.
42) V. Kempter, F. Veith and L. Zehnle: J. Phys. B **8** (1975) 1041.
43) H. D. Hagstrum: Phys. Rev. **89** (1953) 244.
44) S. Thomas and E. B. Pattison: J. Phys. D **3** (1970) 349.
45) A. V. Phelps: *Collision Data Compilation*, unpublished.
46) A. V. Phelps: J. Appl. Phys. **76** (1994) 747.
47) D. Hasselkamp, K. G. Lang, A. Scharmann and N. Stiller: Nucl. Inst. Methods **180** (1981) 349.
48) D. Hasselkamp: *Particle Induced Electron Emission II* (Springer-Verlag, Berlin, 1992) p. 43.
49) H. C. Hayden and N. G. Utterback: Phys. Rev. **135** (1964) A1575.
50) J. P. Boeuf and L. C. Pitchford: J. Phys. D **28** (1995) 2083.
51) D. Marić, K. Kutasi, G. Malović, Z. Donkó and Z. Lj. Petrović: Eur. Phys. J. D **21** (2002) 73.
52) K. Rózsa, A. Gallagher and Z. Donkó: Phys. Rev. E **52** (1995) 913.